Biosensors and Bioelectronics 142 (2019) 111548

Contents lists available at ScienceDirect

Biosensors and Bioelectronics

journal homepage: www.elsevier.com/locate/bios

PtCo nanocubes/reduced graphene oxide hybrids and hybridization chain reaction-based dual amplified electrochemiluminescence immunosensing of antimyeloperoxidase

Wei Yang[a], Qiling Peng[b], Zhen Guo[c], Haiping Wu[b], Shijia Ding[b], Yongjian Chen[a,**], Min Zhao[b,*]

[a] Department of Clinical Laboratory, Zhejiang Provincial People's Hospital, People's Hospital of Hangzhou Medical College, Hangzhou, 310014, China
[b] Key Laboratory of Clinical Laboratory Diagnostics (Ministry of Education), College of Laboratory Medicine, Chongqing Medical University, Chongqing, 400016, China
[c] Department of Clinical Laboratory, Second Affiliated Hospital, School of Medicine, Zhejiang University, Hangzhou, 310009, China

ARTICLE INFO

Keywords:
PtCo nanocubes/reduced graphene oxide
Hybridization chain reaction
Electrochemiluminescence
Immunosensor
Anti-MPO

ABSTRACT

Antimyeloperoxidase (anti-MPO) is regarded as one of the most important circulating autoantibodies for anti-neutrophil cytoplasm antibody (ANCA)-associated vasculitides (AAVs). Hence, it is crucial for highly sensitive detection of anti-MPO to monitor efficacy of AAVs in clinical diagnosis. Herein, a highly sensitive electrochemiluminescence (ECL) immunosensor for anti-MPO detection was constructed by combining reduced graphene oxide-supported PtCo nanocubes hybrids (PtCo@rGO) with hybridization chain reaction (HCR) as signal amplification. Multiple ECL luminophores (Dox-ABEI) prepared by cross-linking of N-(aminobutyl)-N-(ethylisoluminol) (ABEI) and doxorubicin (Dox) were intercalated into dsDNA products of HCR, achieving the effective immobilization of ECL luminophores to obtain strong ECL emission. Benefiting from the efficient catalytic activity of PtCo@rGO toward H_2O_2, the massive the superoxide radical ($O_2^{\bullet-}$) were generated to further react with ABEI for ECL emission. Thus, the designed ECL immunoassay for anti-MPO detection exhibited excellent sensitivity of a concentration variation from 50 fg/mL to 1 ng/mL and a detection limit of 15.68 fg/mL. Importantly, this work proposed an enzyme-free ECL immunoassay with high sensitivity, excellent specificity for protein detection in clinical diagnosis.

1. Introduction

Anti-neutrophil cytoplasm antibody (ANCA)-associated vasculitides (AAVs) are now recognized as a systemic vasculitis of small vessels with a high risk of relapse and life-threatening complications (Nakazawa et al., 2018). Since 1980s, anti-MPO (MPO-ANCAs) has been regarded as one of important serological hallmarks to diagnose AAVs (Guillevin et al., 2014). According to the revised international consensus in 2017 (Bossuyt et al., 2017; Savige et al., 1999), anti-MPO is initially screened by indirect immunofluorescence (IIF), and then verified by enzyme-linked immunosorbent assays (ELISA) to diagnose AAVs. However, IIF and ELISA have been still facing great challenges in clinical practice, such as poor sensitivity and specificity, even requiring skillful operators with complex training (Savige et al., 1999, 2003). Besides, chemiluminescence immunoassay (CLIA) as a popular method in the anti-MPO detection has been developed, which shows higher sensitivity and easier operation in comparison with IIF and ELISA (Mahler et al., 2012). Regrettably, high cost of enzymes used in CLIA increase the medical burden (Roth et al., 2013). Thus, to establish an enzyme-free assay with the advantages of easy manipulation, low cost and high sensitivity for anti-MPO detection is an urgent demand of modern clinical diagnosis.

Electrochemiluminescence (ECL) immunoassay, due to its high sensitivity, excellent specificity and low background, has been widely used in the fields of clinical diagnosis, drug analysis and cellular imaging (Farka et al., 2017; Chen et al., 2010). In ECL system, luminol or its derivatives with high luminescence yield, cheap cost and good biocompatibility become one kind of the most popular luminophores, which is commonly added into the testing buffer for ECL emission. However, there are the shortcomings of waste the reagent and limited luminescence effectiveness. In order to overcome the above-mentioned shortcomings, the efficient immobilization of luminol or its derivatives is a key point to obtain high ECL signal for further greatly improving the sensitivity of the ECL bioassay. Hybridization chain reaction (HCR), which triggered by ssDNA to self-assemble two metastable hairpin

* Corresponding author.
** Corresponding author.
E-mail addresses: lab_cyj@126.com (Y. Chen), zhaomin@cqmu.edu.cn (M. Zhao).

https://doi.org/10.1016/j.bios.2019.111548
Received 14 May 2019; Received in revised form 26 July 2019; Accepted 28 July 2019
Available online 30 July 2019
0956-5663/

probes into long nicked dsDNA products, has been employed as a powerful enzyme-free signal amplification strategy in the bio-analysis applications (Bi et al., 2017; Li et al., 2016a; Li et al., 2019; Cao et al., 2016). Wang's group used HCR-based long dsDNA grafted recognition element as the nanocarrier for doxorubicin (Dox) immobilization *via* intercalation, realizing targeted anticancer drug delivery (Li et al., 2016b). Inspired by the above research, a novel ECL luminophore (Dox-ABEI) prepared by cross-linking of N-(aminobutyl)-N-(ethylisoluminol) (ABEI) and Dox could be anchored onto the dsDNA products of HCR, which could effectively immobilize plenty of ECL luminophores to obtain strong ECL signals.

Bimetallic nanoparticles have received considerable attention in catalysis, fuel cell and biosensing because of their better catalytic performance than that of single-metal components (Koh and Strasser, 2007; Wei et al., 2012; Zhang et al., 2012). Among various bimetallic candidates, Pt-based bimetallic nanoparticles, especially alloying Pt with another transition metals (Co, Fe, Cu, Ni, etc.), possess high catalytic activity, superior biocompatibility and enhanced electron transfer, which hold great promise as efficient catalysts instead of bio-enzymes. However, abundant works have reported that the high-efficiency catalytic performance is closely related to the dispersity, size and shape of active metal nanoparticles (Wang and Yamauchi, 2013). Two-dimensional (2D) graphene sheets with rich surface chemistry, large specific surface area and excellent physical properties (e.g., stability, solubility and conductivity) have been generally developed as pre-eminent support matrixes (Imani et al., 2018; Liu et al., 2011; Sousa et al., 2018; Shi et al., 2019). Especially, the presence of functional groups such as –OH, –COOH on graphene sheets provided sites for metal nanoparticles anchoring and the 2D structure permit large loading of metal nanoparticles with almost no agglomeration contributing to higher dispersion. Therefore, reduced graphene oxide-supported PtCo nanocubes hybrids (PtCo@rGO) have been synthesized by a one-pot hydrothermal method, ensuring the dispersion and loading of PtCo nanocubes to improve the catalytic activity. Besides, the prepared PtCo@rGO hybrids could also be employed as nanocarriers for secondary antibody and ECL luminophores to construct an efficient signal label in ECL immunoassay.

Herein, a dual amplified ECL immunosensor based on PtCo@rGO hybrids and HCR is proposed for highly sensitive detection of anti-MPO. As illustrated in Scheme 1A, firstly, shape-controlled PtCo@rGO hybrids were synthesized by a one-pot hydrothermal method, and then thiol-modified DNA trigger (T_0) and secondary antibody (anti-Ab) were successively assembled on the surface of PtCo@rGO hybrids to form anti-Ab/T_0/PtCo@rGO composites. Moreover, the ECL immunosensor was fabricated by immobilizing antigen MPO on the glassy carbon electrode decorated with Au nanoparticles functionalized MoS_2 (Au@MoS_2) composites. In the presence of anti-MPO, the anti-Ab/T_0/PtCo@rGO composites were assembled onto the surface of modified electrode based on the sandwich immunoreaction, and then the T_0 triggered HCR to form dsDNA products for anchoring massive Dox-ABEI *via* intercalation. Upon the ABEI-H_2O_2 ECL system, the proposed enzyme-free immunosensor has displayed high sensitivity for the detection of anti-MPO, which was attributed to the following two reasons: (i) the synthesized PtCo@rGO hybrids possessed high catalytic efficiency toward H_2O_2 to generate the superoxide radical ($O_2^{\bullet-}$) which further reacted with ABEI for ECL emission, (ii) the proposed HCR could produce long nicked dsDNA products for effectively immobilizing a large of ABEI to obtain strong ECL emission. Meaningfully, this work provided an enzyme-free, sensitive and specific ECL method for anti-MPO detection, which held potential applications in the clinical diagnosis.

2. Experimental

2.1. Reagents and materials

Mouse anti-human myeloperoxidase monoclonal antibody (anti-MPO, target), rabbit anti-mouse IgG (anti-Ab) and human MPO were purchased from Abcam PLC (Cambridge, UK). Prostate specific antigen (PSA), vascular endothelial growth factor (VEGF), carcinoembryonic antigen (CEA), molybdenum sulfide powder (MoS_2), graphene oxide (GO), chloroauric acid ($HAuCl_4{\cdot}3H_2O$), chloroplatinic acid (H_2PtCl_6), tri (2-carboxyethyl) phosphine hydrochloride (TCEP), 97% doxorubicin hydrochloride (Dox), N-(4-aminobutyl)-N-(ethylisoluminol) (ABEI), sodium citrate, glutaraldehyde, glycine, bovine serum albumin (BSA, purity ≥98%), polyvinyl pyrrolidone (PVP, MW: 30,000) and hydrogen peroxide (H_2O_2) were obtained from Sigma-Aldrich (St. Louis, USA). DL20 DNA marker was purchased from Takara (Dalian, China). Gelred nucleic stain was purchased from SenBeiJia Biological Tech. Co., Ltd (Nanjing, China). All oligonucleotide sequences were ordered from Sangon (Shanghai, China), and the sequences were listed in Table S1.

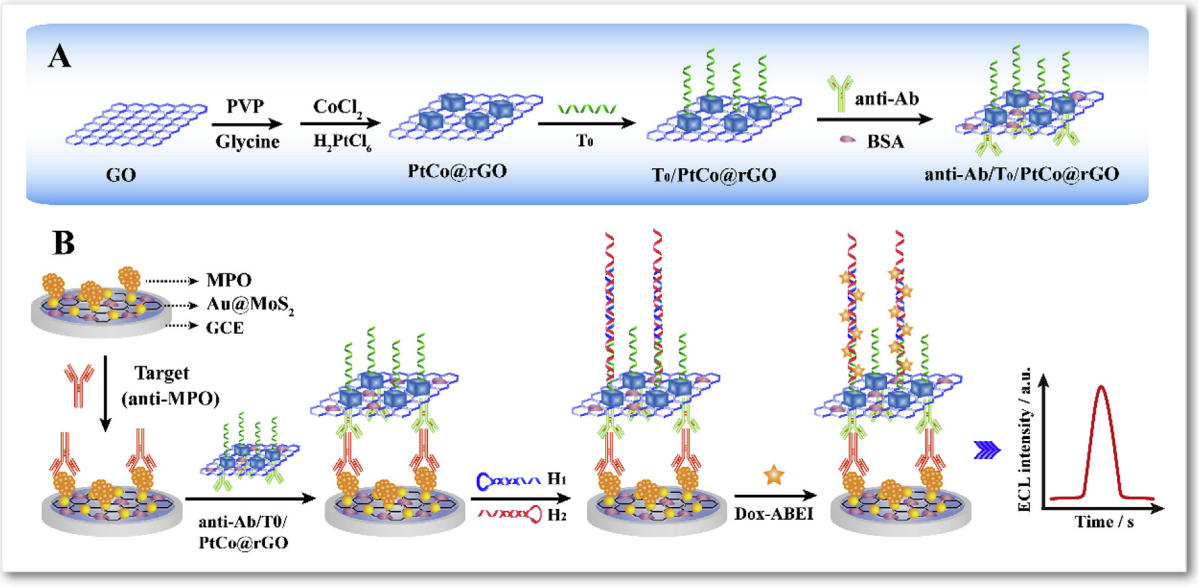

Scheme 1. Schematic illustration of the fabrication process of the ECL immunosensor for anti-MPO detection: (A) the preparation procedure of the anti-Ab/T_0/PtCo@rGO; (B) the construction of the sandwich-type immunosensor.

All other reagents were of analytical grade, and the buffers were prepared using Millipore-Q water (≥18 MΩ, Milli-Q, Millipore, Germany).

2.2. Instruments

The ECL measurements were performed on the MPI-E ECL workstation (Remex, Xi'an, China) with a conventional three-electrode system composed of Pt wire as auxiliary, Ag/AgCl electrode as reference and modified GCE as working electrode, respectively. Electrochemical impedance spectroscopy (EIS) and cyclic voltammetry (CV) were carried out with a CHI 660E electrochemistry workstation (Shanghai Chenhua Instrument, Shanghai, China). Scanning electron microscope (SEM, Hitachi SU8010, Japan) was employed to characterize the nanomaterials. Energy dispersive spectrometer (EDS, Oxford X-MaxN, Britain) was used to analyze the elements of the PtCo@rGO hybrids. The UV-2550 visible spectrophotometer (Shimadzu, Kyoto, Japan) was used to characterize Au@MoS_2 nanosheets. The polyacrylamide gel electrophoresis (PAGE) analysis was carried out on a Bio-Rad electrophoresis analyzer (Bio-Rad, USA).

2.3. Synthesis of Dox-ABEI

The Dox-ABEI complex was prepared according to the previous report (Xie et al., 2016). Firstly, 0.5 mL ABEI solution (0.01 mM) was mixed with 0.5 mL Dox solution (15 mM), and then 0.5 mL glutaraldehyde (1 wt%) as cross-linking agent was dropped into the above mixture with constant stirring for 12 h to obtain the Dox-ABEI complex. The synthetic route of Dox-ABEI compounds was shown in Fig. S1.

2.4. Synthesis of PtCo@rGO hybrids

The PtCo@rGO hybrids were synthesized according to the previous report with slight modification (Qin et al., 2016). 0.8 mg GO was added into 1 mL deionized water under the vigorous ultrasonication for 0.5 h and then, 220 mg PVP was added and stirred for 12 h. After that, 118 mg glycine, 4 mL $CoCl_2$ solution (1.66 mM), 1 mL H_2PtCl_6 solution (20 mM) and 0.5 mL as-prepared GO suspension (PVP-GO) were mixed together and stirred for 30 min, and then sonicated in an ultrasonic bath at room temperature for 5 min. The resultant solution was transferred to a 50 mL Teflon-lined stainless-steel autoclave. The sealed vessel was heated at 200 °C for 9 h and then cooled to room temperature. The resultant products were collected by centrifugation at 9000 rpm for 15 min, and then washed with an ethanol/acetone (volume ratio = 2/1) mixture for three times. The final precipitate (PtCo@rGO) was dispersed in 5 mL deionized water and stored at 4 °C for further use.

2.5. Fabrication of anti-Ab/T_0/PtCo@rGO bioconjugates

180 μL phosphate buffered saline (PBS, 0.01 M, pH 7.4, 137 mM NaCl, 2.7 mM KCl, 8 mM Na_2HPO_4, 1.8 mM KH_2PO_4) containing 5 mM TCEP, 100 μL PtCo/rGO hybrids dispersion, 20 μL thiol-labeled DNA primer (T_0, 100 mM) were mixed and gently stirred for 30 min, and then 200 μL rabbit anti-mouse IgG (anti-Ab, 1 mg/mL) was mixed together and gently shaken for 12 h at 4 °C. As-prepared anti-Ab/T_0/PtCo@rGO was collected by centrifugation for 15 min at 9000 rpm. After that, to prevent nonspecific binding, 200 μL BSA blocking buffer (1.0 wt%) was added into the mixture and stirred at room temperature for 1 h. Finally, the obtained product (anti-Ab/T_0/PtCo@rGO) was centrifuged and washed with PBS for three times to remove free T_0 and anti-Ab, and then dispersed in 500 μL PBS at 4 °C for further use.

2.6. Synthesis of Au@MoS_2 nanosheets

Au@MoS_2 nanosheets were synthesized according to the previous literature with some modification (Su et al., 2014). 10 mL MoS_2 (20 μg/mL), 120 μL sodium citrate (100 mM), 20 μL Tween-80 (100 mM) and 100 μL $HAuCl_4$ (28.5 mM) solutions were mixed together and stirred vigorously. Next, the obtained mixture was heated to 60 °C for 5 min and then naturally cooled down to room temperature. Finally, the product of Au@MoS_2 nanosheets was centrifuged (7000 rpm, 20 min) to remove excess reagents. After that, the supernatant was discarded and the precipitates (Au@MoS_2 nanosheets) were dispersed in 5 mL deionized water.

2.7. Construction of ECL immunosensor

Firstly, the bare GCE (3 mm in diameter) was polished to a mirror-like surface using 0.3 μm Al_2O_3 slurry, and then the electrode was ultrasonically washed with deionized water and ethanol successively for 10 min. Next, the electrode was dried under N_2 flush. 10 μL Au@MoS_2 nanosheets solution was dropped onto the surface of clean GCE to form Au@MoS_2 film when the solvent evaporated at 37 °C. The obtained electrode was denoted as Au@MoS_2/GCE. After that, 10 μL antigen MPO (200 μg/mL) dispersion was added onto the Au@MoS_2/GCE and incubated overnight at 4 °C. Next, 10 μL BSA blocking buffer (1.0 wt%) was added onto the MPO/Au@MoS_2/GCE and incubated at room temperature for 1 h to eliminate nonspecific binding sites of the modified electrode. Ultimately, the electrode (BSA/MPO/Au@MoS_2/GCE) was rinsed with 0.01 M PBS (pH 7.4) for further use.

2.8. ECL detection of anti-MPO

Different concentrations of anti-MPO (standard solutions or serum samples) were incubated with the prepared immunosensor (BSA/MPO/Au@MoS_2/GCE) at room temperature for 1 h. Subsequently, the modified electrode was further incubated with 10 μL as-prepared anti-Ab/T_0/PtCo@rGO bioconjugates at 37 °C for 1 h. Next, the DNA hairpins mixtures (H_1 and H_2) were dropped onto the surface of the modified electrode at 37 °C for 90 min. Then, 10 μL Dox-ABEI complex was added into the above modified electrode and reacted at room temperature for 4 h to adequately intercalate into dsDNA (formed by HCR). After each step, the modified electrode surface was washed thoroughly with 0.01 M PBS (pH 7.4) to eliminate unbound substance. Finally, the ECL measurement was carried out under potential scanning from 0 to 0.8 V at a scan rate of 0.1 V/s in 4 mL 0.01 M air-saturated PBS (pH 7.4) containing 3 mM H_2O_2, and the photomultiplier tube voltage was set at 800 V.

3. Results and discussion

3.1. Characterization of PtCo@rGO hybrids

The morphology, size and elemental composition of the as-synthesized nanomaterials were characterized by high-resolution transmission electron microscopy (HRTEM), scanning electron microscope (SEM) and STEM-EDS elemental mapping. As HRTEM results shown in Fig. 1A, well-dispersed and uniform-sized PtCo nanocubes with an average apex-to-apex diameter of 39.7 ± 3.3 nm (Fig. 1A, inset) were distributed on the surface of rGO. Moreover, Fig. 1B illustrated a clear structure of PtCo nanocube. Additionally, the SEM results of GO, PVP-functionalized GO and PtCo@rGO hybrids were displayed in Fig. S2. Comparing to the wrinkled thin paper-like GO (Fig. S2A), PVP-functionalized GO were even more wrinkled (Fig. S2B). When PtCo nanocubes were *in situ* synthesized on the surface of rGO, the SEM image demonstrated well-dispersed and uniform-sized PtCo nanocubes with a grain diameter of 40 nm on the surface of rGO (Fig. S2C). The SEM results were consistent with the HRTEM results.

To confirm the chemical compositions of PtCo@rGO hybrids, STEM-EDS elemental mapping analysis was performed. As shown in Fig. 1C-G, the Pt and Co element were evenly distributed onto the entire nanocube structure, indicating that the PtCo alloys on the rGO were synthesized successfully. EDS elemental analysis was also performed. As shown in

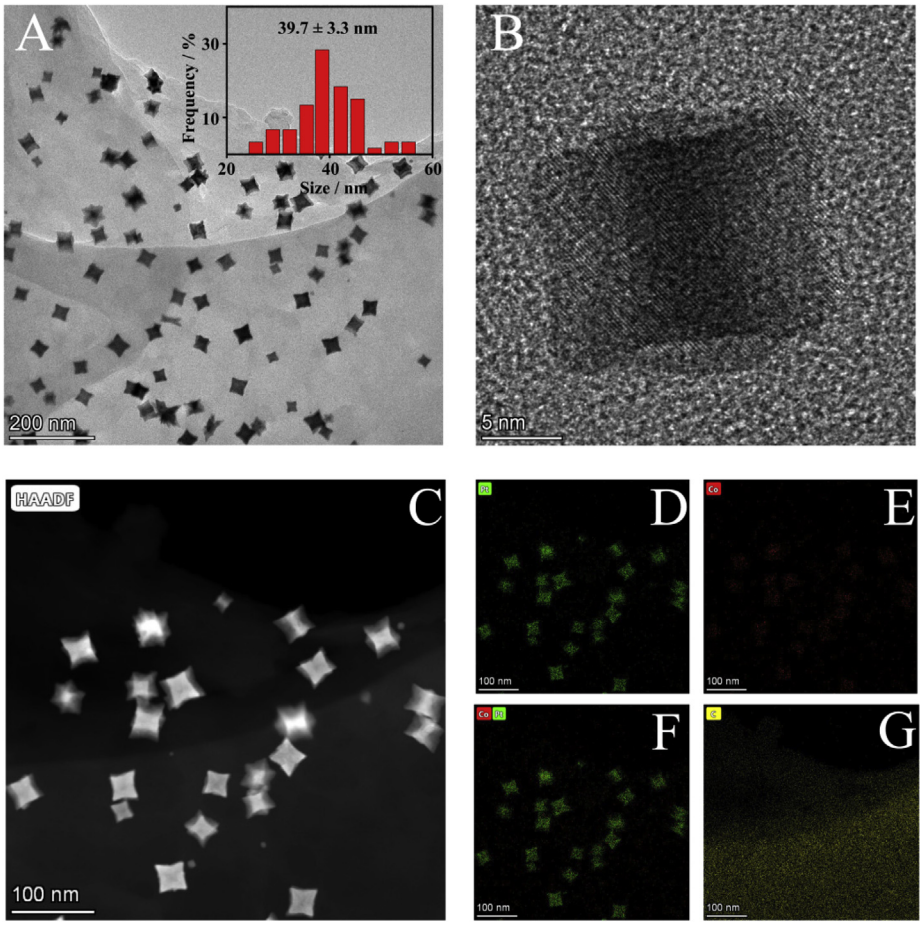

Fig. 1. Structural and compositional analyses of the PtCo/rGO nanocubes. (A) TEM and size-distribution histogram of PtCo/rGO nanocubes. Scale bar is 200 nm; (B) HRTEM of PtCo/rGO nanocubes. Scale bar is 5 nm; (C) The high-angle annular dark-field (HAADF)-STEM image of PtCo/rGO nanocubes. Scale bar is 100 nm. (D–G) STEM-EDS elemental mapping of PtCo/rGO nanocubes. Scale bar is 100 nm.

Fig. S2D, the appearance of the Pt and Co element peaks indicated that the PtCo alloys on the rGO were synthesized successfully.

UV–vis absorption spectroscopy was employed to further investigate the as-synthesized PtCo@rGO hybrids. As shown in Fig. S3B, when GO was functionalized by PVP, the absorption peak of GO shifted from 228 nm to 218 nm (curve a *vs* curve b). The peak shift would mean that there was an interaction between PVP and GO due to the abundant C–O, C═O and O–H functional groups and the high surface area of GO (Qin et al., 2016). Additionally, typical UV–vis spectrum of PtCo@rGO hybrids displayed an absorption shoulder at 267 nm, indicating that GO was reduced and the electronic conjugation within the graphene was restored (Wang et al., 2015). Moreover, Raman spectroscopy was also used to characterize the as-synthesized PtCo@rGO hybrids and the results were exhibited in Fig. S3C.

3.2. Characterization of MoS_2 and Au@MoS_2 nanosheets

The SEM was employed to characterize the as-prepared Au@MoS_2 nanosheets. Fig. 2A showed SEM image of MoS_2 nanosheets, which exhibited a typical layer-like structure with diameter of ~500 nm. When Au nanoparticles (AuNPs) were *in situ* reduced on the surface of MoS_2 nanosheets, it could be seen that AuNPs with the diameter of ~10 nm were evenly dispersed on the surface of MoS_2 nanosheets (Fig. 2B). TEM was also used to characterize MoS_2 and Au@MoS_2 nanosheets in Fig. 2C and D. It could be seen that the Au nanoparticles with an average diameter of 8.1 ± 0.7 nm (Fig. 2D, inset) were distributed on the surface of MoS_2 nanosheets. These results were consistent with SEM results.

Besides, UV–vis absorption spectroscopy was also used to characterize MoS_2 and Au@MoS_2 nanosheets (Fig. S3D). MoS_2 nanosheets showed two absorption peaks at wavelengths of 233 nm and 284 nm, which was consistent with the reported works (Liu et al., 2014). When the AuNPs were *in situ* reduced onto the surface of MoS_2 nanosheets, a characteristic absorption peak of AuNPs at 525 nm was present, which could be assigned to the surface plasmon resonance peak of AuNPs (Devi et al., 2018; Su et al., 2014). Thus, the results from UV–vis spectra further confirmed that the AuNPs were successfully prepared over MoS_2 nanosheets.

3.3. Gel electrophoresis characterization of HCR

The HCR were analyzed by Gel electrophoresis (12% native polyacrylamide gel electrophoresis) in running buffer (TBE, 89 mM Tris, 89 mM boric acid, 2 mM EDTA) for 60 min at 100 V constant voltages (Sun et al., 2019). As shown in Fig. 3A, the DNA ladder marker, trigger (T_0), hairpin probe 1 (H_1), hairpin probe 2 (H_2), T_0+H_1, H_1+H_2, and $T_0+H_1+H_2$ displayed different bright bands in gel electrophoresis, respectively. As expected, T_0, H_1 and H_2 showed a single band, as indicated in lane 1, lane 2 and lane 3, respectively. When H_1 was incubated with trigger T_0, we could clearly observe a new downstream band in lane 4 except bands for T_0 and H_1. This demonstrated that T_0 initiated the cross-opening of H_1 to form dsDNA. However, a new band was absent as shown in lane 5 when H_1 and H_2 were incubated together. It could be concluded that two species of H_1 and H_2 could coexist metastably in the absence of trigger T_0. As expected, ladder bands appeared in lane 6 when T_0 was added into the mixture of H_1 and H_2. This was attributed that T_0 opened H_1, and then the newly exposed domain of H_1 acted as another initiator to interact with the sticky end of H_2. Finally, nicked dsDNA products were obtained by the cross-opening of H_1 and H_2 until the supply of H_1 or H_2 was exhausted (Bi et al., 2017).

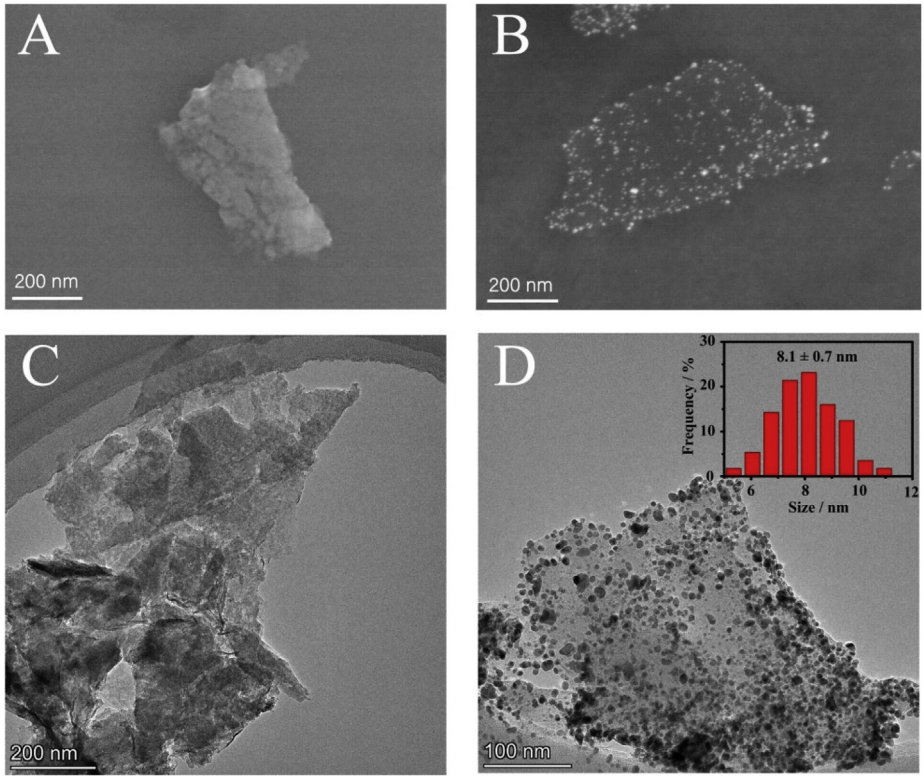

Fig. 2. SEM images of (A) MoS_2 and (B) Au@MoS_2 nanosheets. TEM images of (C) MoS_2 and (D) Au@MoS_2 nanosheets.

3.4. Comparison of the ECL responses with different nanoparticles

In order to explore the superiority of PtCo@rGO hybrids towards the ABEI-H_2O_2 ECL system, the analytical performance of different nanoparticles including Pt@rGO, PtCo and PtCo@rGO hybrids had been compared in the whole of ECL immunosensor system. Specifically, the developed immunosensors (BSA/MPO/Au@MoS_2/GCE) were successively incubated with 1 ng/mL of anti-MPO, three different nanomaterials, the DNA hairpins mixtures and Dox-ABEI. As the results shown in Fig. 3B, a high ECL signal about 6684 a.u was observed from the Pt@rGO-based ECL immunosensor (curve a). However, a relatively low ECL signal about 5123 a.u. was observed from PtCo-based ECL immunosensor (curve b). As expected, a highest ECL signal about 9099 a.u. was obtained from the PtCo@rGO-based ECL immunosensor (curve c), which was higher than that of Pt@rGO and PtCo-incubated ECL immunosensors. These results showed that the bimetallic PtCo NPs had higher catalytic activity than that of monometallic Pt NPs and rGO had large specific surface area to support massive PtCo NPs. As discussed above, PtCo@rGO hybrids had excellent electrocatalytic activity towards ABEI-H_2O_2 ECL system for signal amplification. Moreover, localized surface plasmon resonance (LSPR) of PtCo@rGO hybrids towards ABEI-H_2O_2 system was also studied by numerical calculation of Maxwell's equations (Fig. S5).

3.5. Electrochemical characterization of the ECL immunosensor

Electrochemical impedance spectroscopy (EIS) was performed to monitor the impedance changes of during the fabrication process of electrodes. These electrodes were evaluated by EIS in 0.01 M PBS (pH 7.4) containing 5 mM $K_3[Fe(CN)_6]$, 5 mM $K_4[Fe(CN)_6]$ and 0.1 M KCl. The electron-transfer resistance was exhibited by the diameter of semicircle. When the electron transfer was accelerated, a smaller semicircle diameter was achieved (Chen et al., 2010). As shown in Fig. 4A, when Au@MoS_2 nanosheets were modified onto the surface of GCE, a smaller semicircle diameter was observed compared with bare GCE (curve a *via* curve b), attributing to the excellent electroconductivity of Au@MoS_2 nanosheets. Nevertheless, when the MPO (curve c) and BSA (curve d) were sequentially assembled onto the Au@MoS_2-modified GCE, the semicircle diameters successively increased. After the modified electrode incubated with target anti-MPO, the electron transfer was further limited (curve e). These results were attributed that the biomolecules restricted the electron transfer.

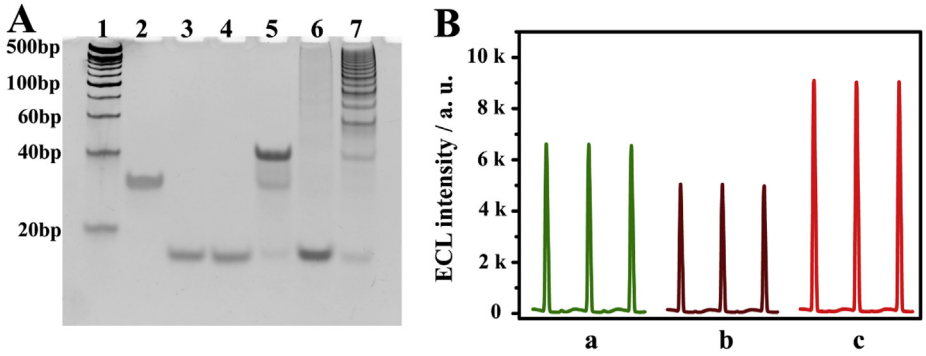

Fig. 3. (A) Gel electrophoresis characterization of HCR process. Lane M: 20 bp DNA ladder marker; lane 1: 1 μM T_0; lane 2: 1 μM H_1; lane 3: 1 μM H_2; lane 4: 1 μM T_0 + 1 μM H_1; lane 5: 1 μM H_1 + 1 μM H_2; lane 6: 0.5 μM T_0 + 1 μM H_1 + 1 μM H_2. (B) ECL responses of Pt@rGO (a), PtCo (b) and PtCo@rGO hybrids (c) incubated with 1 ng/mL of anti-MPO in 4 mL 0.01 M PBS (pH 7.4) containing 5.0 mM H_2O_2 with a potential from 0 to 0.8 V at a scan rate of 0.1 V/s.

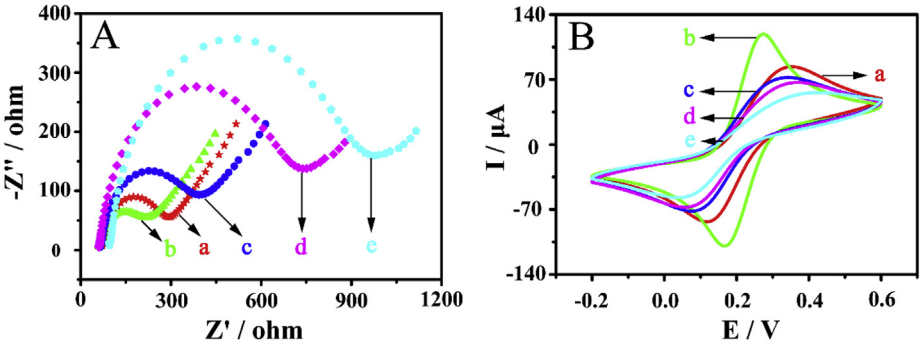

Fig. 4. (A) EIS and (B) CV curves of bare GCE (a), $Au@MoS_2$/GCE (b), MPO/$Au@MoS_2$/GCE (c), BSA/MPO/$Au@MoS_2$/GCE (d), anti-MPO/BSA/MPO/$Au@MoS_2$/GCE (e), respectively, in 0.01 M PBS (pH 7.4) containing 5 mM $K_3[Fe(CN)_6]$, 5 mM $K_4[Fe(CN)_6]$ and 0.1 M KCl. EIS measurements were carried out with a frequency range of 0.1–100 kHz and amplitude of 50 mV. The CV experiments were scanned from −0.2–0.6 V vs Ag/AgCl reference at a scan rate of 0.1 V/s.

On the other hand, the cyclic voltammetry (CV) as another effective tool was adopted to characterize the fabricated electrodes. Fig. 4B displayed the CV curves of various modified electrodes in the same electrolyte of EIS. A pair of redox was observed due to the oxidation and reduction of $Fe(CN)_6^{4-/3-}$. As curve a and curve b shown in Fig. 4B, the peak current increased compared with bare GCE when $Au@MoS_2$ was modified on the electrode. Subsequently, the peak current successively decreased after MPO and BSA were immobilized on the modified electrode, separately (curve c and curve d). As expected, the peak current further decreased with the binding between MPO and anti-MPO (curve e). These CV results were well-consistent with that of EIS, indicating that the ECL immunosensor was successfully constructed.

3.6. Optimization of the reaction conditions

In order to obtain the optimal performance of the ECL immunosensor, we optimized several vital conditions, including the dilution ratio of PtCo/rGO hybrids, the reaction time of Dox-AEBI, the incubation time of anti-MPO and the concentration of H_2O_2, respectively. Fig. S7A showed the influence of the dilution ratio of PtCo/rGO hybrids on the ECL responses of the biosensor. It could be seen that the ECL intensity gradually increased with the dilution ratio of PtCo/rGO hybrids until the ECL intensity reached maximum value at 5 times dilution. Thus, 5 times dilution of PtCo/rGO hybrids was chosen as the optimum reaction condition in this study. Fig. S7B illustrated the effect of Dox-AEBI reaction time on the ECL responses of the biosensor. When reaction time increased, more Dox-AEBI molecules could be intercalated into dsDNA until the ECL intensity gave rise to a roughly flat plateau in 240 min. Therefore, 240 min was chosen as the optimum reaction time in this study. Besides, the incubation time of anti-MPO was also investigated to evaluate the performance of the ECL immunosensor. As displayed in Fig. S7C, the ECL intensity gradually increased with incubation time until the ECL intensity reached to saturation in 60 min. Therefore, 60 min was chosen as the optimum incubation time of anti-MPO in this study. Finally, the concentration of H_2O_2 was also optimized. As shown in Fig. S7D, the ECL intensity was enhanced when the H_2O_2 concentration was increased from 0.05 to 8 mM. When the H_2O_2 concentration reached 3 mM, the ECL intensity had no obvious change. Thus, the optimal concentration of H_2O_2 was 3 mM.

3.7. Analytical performance of the ECL immunosensor

For the purpose of quantitative analysis, the amounts of anti-MPO in solution were determined by the ECL immunosensor under the optimal conditions. Concretely, the developed ECL immunosensor was incubated with different concentrations of anti-MPO. As shown in Fig. 5A, ECL intensities progressively increased with anti-MPO concentrations in the range of 0.05–1000 pg/mL. And the ECL intensity was plotted as function of lg $C_{anti\text{-}MPO}$ illustrated in Fig. 5B. The fitted linear equation was $I = 4196.80 + 1850.36 \lg C_{anti\text{-}MPO}$ ($R^2 = 0.9950$) with a detection limit (LOD) of 15.68 fg/mL. This proposed ECL immunosensor for anti-MPO detection exhibited excellent analytical performance, which was not only the high electrocatalytic activity and LSPR of PtCo@rGO towards ABEI-H_2O_2 system but also the large immobilization of luminophore ABEI by the HCR amplification strategy.

To verify the specificity, cross-reactivity studies of the ECL immunosensor was tested against BSA, AFP, VEGF, PSA and the mixture containing anti-MPO (Fig. 5C). Under the optimal conditions, 1 pg/mL anti-MPO and other interfering proteins were incubated with the ECL immunosensor, respectively. Compared to the interfering proteins, anti-MPO showed very high response to the ECL immunosensor. These results indicated that the designed ECL immunosensor had a good specificity.

Moreover, the stability of the ECL immunosensor was another key parameter. The anti-MPO at 1000 pg/mL with 10 consecutive cycles was measured to evaluate the stability of immunosensor. As displayed in Fig. 5D, the relative standard deviation (RSD) value was as low as 3.7%, exhibiting an acceptable stability. Additionally, long-term stability of ECL immunosensor for anti-MPO detection was evaluated by storing BSA/MPO/$Au@MoS_2$ electrodes at 4 °C (0, 1, 2, 4, 6, 8 and 10 days) and then successively incubating with anti-MPO (1000 pg/mL), anti-Ab/T_0/PtCo@rGO bioconjugates, DNA hairpins mixtures and Dox-ABEI. As shown in Fig. S8, the ECL intensity reduced gradually and retained 90.71% of its initial intensity after 10 days, suggesting that the long-term stability of ECL immunosensor was acceptable.

3.8. Detection of anti-MPO in real samples

Recovery experiments were executed for clinical serum samples to further evaluate the applicability of the ECL immunosensor. Different concentrations of anti-MPO were added in normal human serum (50% diluted by PBS solution). The concentrations of anti-MPO in human serum could be accurately determined by fitted linear equation in Fig. 5B. As displayed in Table 1, the recoveries were obtained from 94.0% to 105.4% with the RSD of 0.5%–2.1% (n = 3), indicating that the designed ECL immunosensor had a great potential application for anti-MPO detection in clinical analysis.

4. Conclusion

In summary, a highly sensitive enzyme-free ECL immunoassay for determination of anti-MPO has been successfully constructed based on the dual amplification strategies of PtCo@rGO and HCR. Significantly, the prepared PtCo@rGO not only exhibited high catalytic capacity towards ABEI-H_2O_2 ECL system to amplify ECL signal, but also employed as excellent nanocarriers for secondary antibody and ECL luminophores to construct an efficient signal label. Besides, HCR-based non-enzymatic isothermal amplification strategy was designed to effectively immobilize the massive ABEI for ECL signal amplification. On the basis of PtCo@rGO and HCR, the developed ECL immunoassay for anti-MPO detection showed prominent sensitivity with LOD down to 15.68 fg/mL, which provided a promising multifunctional platform for clinical diagnosis of ANCA-associated vasculitis or biomarkers (e.g., proteins,

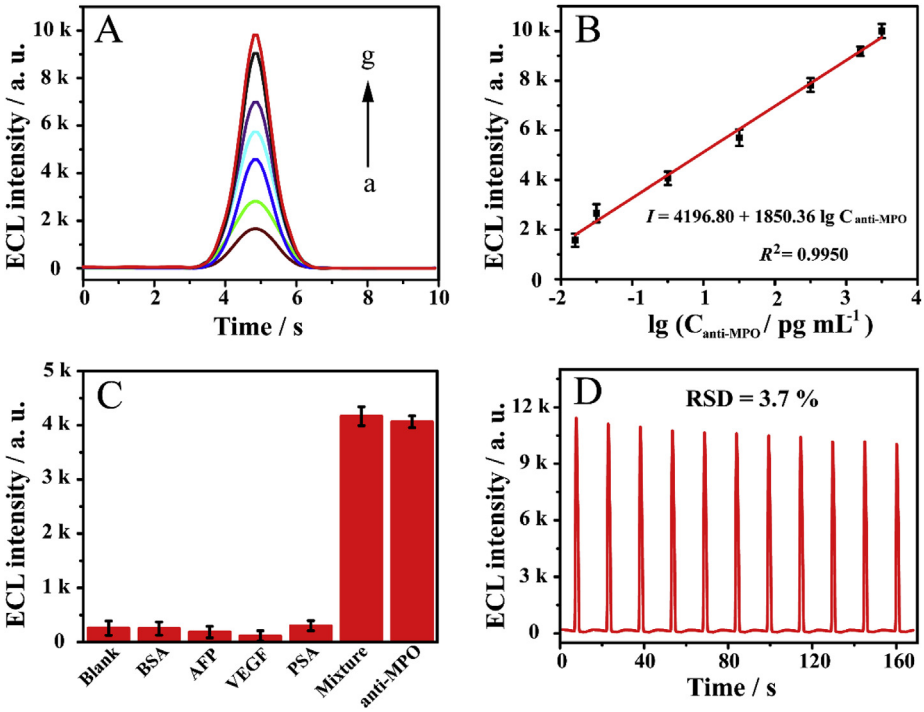

Fig. 5. (A) ECL intensity of the proposed immunosensor with 0.05, 0.1, 1.0, 10, 100, 500 and 1000 pg/mL of anti-MPO. (B) Calibration plot of the ECL intensities vs. the logarithm of anti-MPO concentrations. (C) The cross-reactivity of the ECL immunosensor against other interfering proteins: 50 pg/mL BSA, 20 pg/mL AFP, 10 pg/mL VEGF, 30 pg/mL PSA and their mixture (50 pg/mL BSA, 20 pg/mL AFP, 10 pg/mL VEGF, 30 pg/mL PSA and 1 pg/mL anti-MPO). (D) Stability of the proposed ECL immunosensor incubated with 1000 pg/mL anti-MPO. Inset: ECL experiments conditions were conducted in 4 mL 0.01 M PBS (pH 7.4) containing 3.0 mM H_2O_2 with a potential from 0 to 0.8 V at a scan rate of 0.1 V/s.

Table 1
Determination of anti-MPO in normal serum samples by the designed ECL immunosensor.

Standard solution (fg/mL)	ECL intensity (a.u.)	Calculated (fg/mL)	Recovery (%)	RSD (%)
30.0	1421.0	31.6	105.4	1.5
120.0	2463.7	115.7	96.4	1.9
250.0	3072.7	246.9	98.8	1.3
5.00×10^3	5440.3	4.70×10^3	94.0	0.5

peptides, biomolecules).

Declaration of interests

The authors declare that they have no known competing financial interests or personal relationships that could have appeared to influence the work reported in this paper.

CRediT authorship contribution statement

Wei Yang: Conceptualization, Formal analysis, Writing - original draft. **Qiling Peng:** Writing - review & editing, Software. **Zhen Guo:** Data curation. **Haiping Wu:** Methodology, Investigation. **Shijia Ding:** Project administration, Resources. **Yongjian Chen:** Conceptualization, Funding acquisition. **Min Zhao:** Project administration, Visualization, Writing - review & editing.

Acknowledgements

This research was supported by the National Science and Technology Major Project of the Ministry of Science and Technology of China (No. 2018ZX10732202), Zhejiang Provincial Health Bureau (No. 2017KY218), the National Natural Science Foundation of China (No. 21804015) and the Natural Science Foundation Project of CQ CSTC (No. cstc2018jcyjAX0206).

Appendix A. Supplementary data

Supplementary data to this article can be found online at https://doi.org/10.1016/j.bios.2019.111548.

References

Bi, S., Yue, S., Zhang, S., 2017. Hybridization chain reaction: a versatile molecular tool for biosensing, bioimaging, and biomedicine. Chem. Soc. Rev. 46 (14), 4281–4298.
Bossuyt, X., Cohen, Tervaert, J.W., Arimura, Y., Blockmans, D., Flores-Suárez, L.F., Guillevin, L., Hellmich, B., Jayne, D., Jennette, J.C., Kallenberg, C.G.M., Moiseev, S., Novikov, P., Radice, A., Savige, J.A., Sinico, R.A., Specks, U., van Paassen, P., Zhao, M.H., Rasmussen, N., Damoiseaux, J., Csernok, E., 2017. Revised 2017 international consensus on testing of ANCAs in granulomatosis with polyangiitis and microscopic polyangiitis. Nat. Rev. Rheumatol. 13 (11), 683–692.
Cao, Y., Han, P., Wang, Z., Chen, W., Shu, Y., Xiang, Y., 2016. Binding-regulated click ligation for selective detection of proteins. Biosens. Bioelectron. 78, 100–105.
Chen, J., Zhang, J., Yang, H., Fu, F., Chen, G., 2010. A Strategy for development of electrochemical dna biosensor based on site-specific DNA cleavage of restriction endonuclease. Biosens. Bioelectron. 26 (1), 144–148.
Devi, R., Gogoi, S., Barua, S., Sankar Dutta, H., Bordoloi, M., Khan, R., 2018. Electrochemical detection of monosodium glutamate in foodstuffs based on Au@ MoS_2/chitosan modified glassy carbon electrode. Food Chem. 276, 350–357.
Farka, Z., Jurík, T., Kovář, D., Trnková, L., Skládal, P., 2017. Nanoparticle-based immunochemical biosensors and assays: recent advances and challenges. Chem. Rev. 117 (15), 9973–10042.
Guillevin, L., Pagnoux, C., Karras, A., Khouatra, C., Aumaître, O., Cohen, P., Maurier, F., Decaux, O., Ninet, J., Gobert, P., Quémeneur, T., Blanchard-Delaunay, C., Godmer, P., Puéchal, X., Carron, P.L., Hatron, P.Y., Limal, N., Hamidou, M., Ducret, M., Daugas, E., Papo, T., Bonnotte, B., Mahr, A., Ravaud, P., Mouthon, L., 2014. Rituximab versus azathioprine for maintenance in ANCA-associated vasculitis. N. Engl. J. Med. 42 (4), 1771–1780.
Imani, R., Mohabatpour, F., Mostafavi, F., 2018. Graphene-based nano-carrier modifications for gene delivery applications. Carbon 140, 569–591.
Koh, S., Strasser, P., 2007. Electrocatalysis on Bimetallic Surfaces: modifying catalytic reactivity for oxygen reduction by voltammetric surface dealloying. J. Am. Chem. Soc. 42 (129), 12624–12625.
Li, J., Liu, S., Sun, L., Li, W., Zhang, S.Y., Yang, S., Li, J., Yang, H.H., 2016a. Amplified visualization of protein-specific glycosylation in Zebrafish via proximity-induced hybridization chain reaction. J. Am. Chem. Soc. 140 (48), 16589–16595.
Li, W., Yang, X., He, L., Wang, K., Wang, Q., Huang, J., Liu, J., Wu, B., Xu, C., 2016b. Self-assembled DNA nanocentipede as multivalent drug carrier for targeted delivery. ACS Appl. Mater. Interfaces 8 (39), 25733–25740.
Li, X., Shen, J., Wu, C., Wu, K., 2019. Ball-mill-exfoliated graphene: tunable electrochemistry and phenol sensing. Small, e1805567.
Liu, Q., Shi Sun, J., Wang, T., Zeng, L., Jiang, G., 2011. Graphene and graphene oxide sheets supported on silica as versatile and high-performance adsorbents for solid--phase extraction. Angew Chem. Int. Ed. Engl. 50, 5913–5917.

Liu, T., Wang, C., Gu, X., Gong, H., Cheng, L., Shi, X., Feng, L., Sun, B., Liu, Z., 2014. Drug delivery with PEGylated MoS_2 nano-sheets for combined photothermal and chemotherapy of cancer. Adv. Mater. 26, 3433–3440.

Mahler, M., Radice, A., Yang, W., Bentow, C., Seaman, A., Bianchi, L., Sinico, R.A., 2012. Development and performance evaluation of novel chemiluminescence assays for detection of Anti-PR3 and Anti-MPO antibodies. Clin. Chim. Acta 413 (7–8), 719–726.

Nakazawa, D., Masuda, S., Tomaru, U., Ishizu, A., 2018. Pathogenesis and therapeutic interventions for ANCA-associated vasculities. Nat. Rev. Rheumatol. 15 (2), 91–101.

Qin, Y., Zhang, X., Dai, X., Sun, H., Yang, Y., Li, X., Shi, Q., Gao, D., Wang, H., Yu, N.F., Sun, S.G., 2016. Graphene oxide-assisted synthesis of Pt-Co alloy nanocrystals with high-index facets and enhanced electrocatalytic properties. Small 12, 524–533.

Roth, A.J., Ooi, J.D., Hess, J.J., Timmeren, M.M., Berg, E.A., Poulton, C.E., McGregor, J., Burkart, M., Hogan, S.L., Hu, Y., Winnik, W., Nachman, P.H., Stegeman, C.A., Niles, J., Heeringa, P., Kitching, A.R., Holdsworth, S., Jennette, J.C., Preston, G.A., Falk, R.J., 2013. Epitope specificity determines pathogenicity and detectability in ANCA-associated vasculitis. J. Clin. Investig. 123 (4), 1773–1783.

Savige, J., Gillis, D., Benson, E., Davies, D., Esnault, V., Falk, R.J., Paspaliaris, B., 1999. International consensus statement on testing and reporting of antineutrophil cytoplasmic antibodies (ANCA). Am. J. Clin. Pathol. 111 (4), 507–513.

Savige, J., Dimech, W., Fritzler, M., Goeken, J., Hagen, E.C., Jennette, J.C., McEvoy, R., Pusey, C., Pollock, W., Trevisin, M., Wiik, A., Wong, R., 2003. Addendum to the international consensus statement on testing and reporting of antineutrophil cytoplasmic antibodies. quality control guidelines, comments, and recommendations for testing in other autoimmune diseases. Am. J. Clin. Pathol. 120 (3), 312–318.

Shi, L., Mu, C., Gao, T., Chai, W., Sheng, A., Chen, T., Yang, J., Zhu, X., Li, G., 2019. Rhodopsin-like ionic gate fabricated with graphene oxide and isomeric dna switch for efficient photocontrol of ion transport. J. Am. Chem. Soc. 141 (20), 8239–8243.

Sousa, M.D., Luna, L., Fonseca, L.C., Giorgio, S., Alves, O.L., 2018. Folic-acid-functionalized graphene oxide nanocarrier: synthetic approaches, characterization, drug delivery study, and antitumor screening. ACS Nano 1 (2), 922–932.

Su, S., Zhang, C., Yuwen, L., Chao, J., Zuo, X., Liu, X., Wang, L., 2014. Creating SERS hot spots on MoS_2 nanosheets with *in situ* grown gold nanoparticles. ACS Appl. Mater. Interfaces 6 (21), 18735–18741.

Sun, H., Wu, S., Zhou, X., Zhao, M., Wu, H., Luo, R., Ding, S.J., 2019. Electrochemical sandwich immunoassay for insulin detection based on the use of gold nanoparticle-modified MoS_2 nanosheets and the hybridization chain reaction. Mikrochim. Acta 186, 6.

Wang, L., Yamauchi, Y., 2013. Metallic nanocages: synthesis of bimetallic Pt − Pd hollow nanoparticles with dendritic shells by selective chemical etching. J. Am. Chem. Soc. 135, 16762–16765.

Wang, L., Yang, R., Wang, H., Li, J.J., Qu, L.B., Harrington, P.D.B., 2015. High-selective and sensitive voltammetric sensor for butylated hydroxyanisole based on AuNPs-PVP-graphene nanocomposites. Talanta 138, 169–175.

Wei, Z., Sun, J., Li, Y., Datye, A.K., Wang, Y., 2012. Bimetallic catalysts for hydrogen generation. Chem. Soc. Rev. 24 (41), 7994–8008.

Xie, S., Dong, Y., Yuan, Y., Chai, Y., Yuan, R., 2016. Ultrasensitive lipopolysaccharides detection based on doxorubicin conjugated N-(Aminobutyl)-N-(ethylisoluminol) as electrochemiluminescence indicator and self-assembled tetrahedron DNA dendrimers as nanocarriers. Anal. Chem. 88 (10), 5218–5224.

Zhang, H., Jin, M.S., Xia, Y.N., 2012. Enhancing the catalytic and electrocatalytic properties of Pt-based catalysts by forming bimetallic nanocrystals with Pd. Chem. Soc. Rev. 41, 8035–8049.